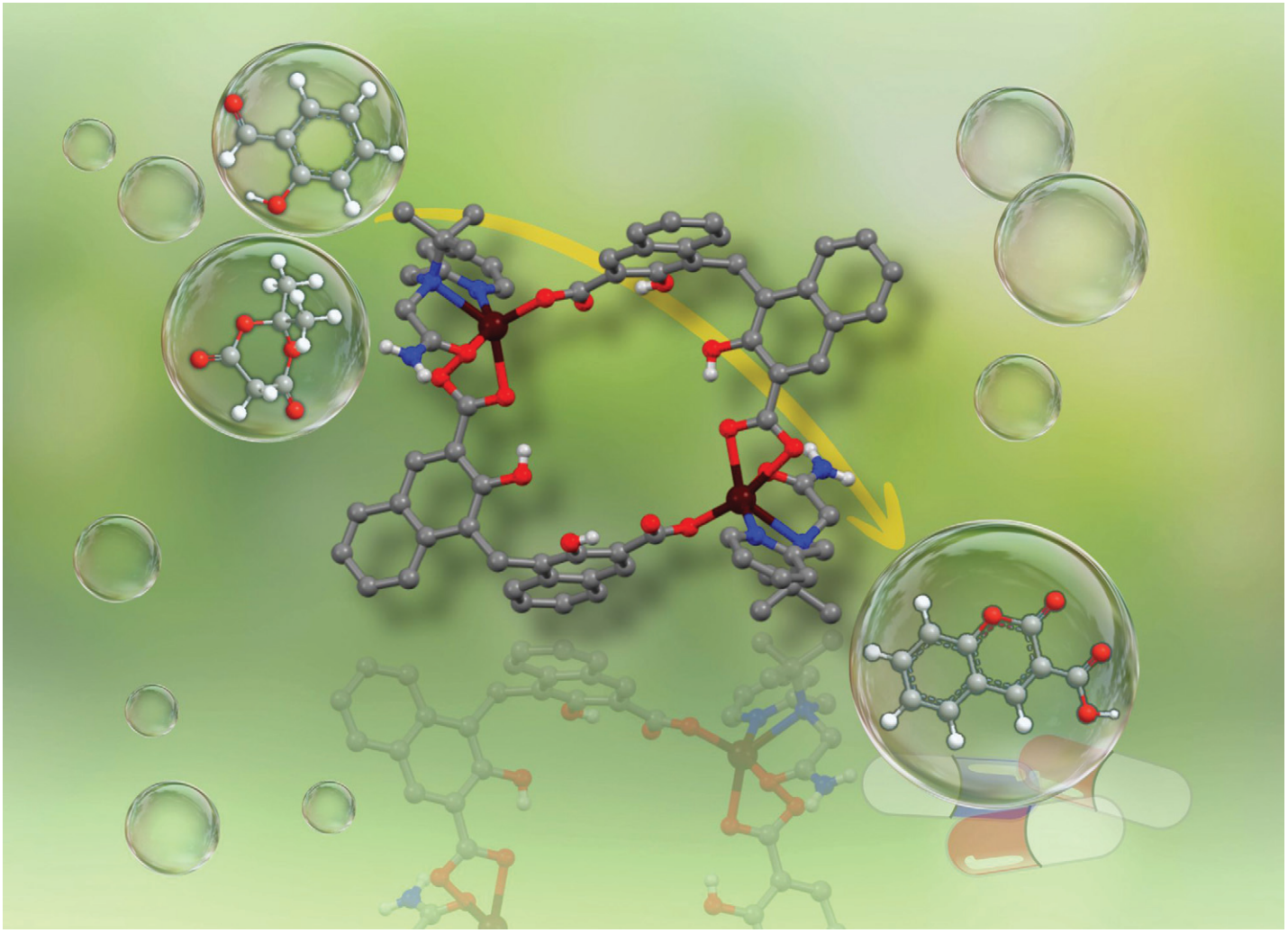

Showcasing research from Professor Sanjay Mandal's laboratory, Department of Chemical Sciences, Indian Institute of Science Education and Research Mohali, Punjab, India.

Synthesis of metal–organic rectangles decorated with primary amide groups for the synergistic Lewis acid and Brønsted base heterogeneous catalysis

This picture depicts the single crystal structure and utilization of molecular rectangles consisting of Lewis acidic metal centres (Zn or Cd) and free NH_2 groups of coordinated primary amide groups acting as Bronsted basic sites in the synthesis of a wide range of coumarin-3-carboxylic acids (C-3-CAs) from the Knoevenagel intramolecular cyclization tandem reaction between salicylaldehyde derivatives and Meldrum's acid under ambient conditions in a green solvent such as methanol.

Image reproduced by permission of Sanjay Mandal from *Catal. Sci. Technol.*, 2025, **15**, 6379.

As featured in:

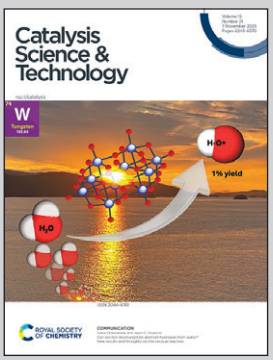

See Alokananda Chanda and Sanjay K. Mandal, *Catal. Sci. Technol.*, 2025, **15**, 6379.

ROYAL SOCIETY OF CHEMISTRY

rsc.li/catalysis

Registered charity number: 207890

Catalysis Science & Technology

ROYAL SOCIETY OF CHEMISTRY

PAPER

View Article Online
View Journal | View Issue

Cite this: *Catal. Sci. Technol.*, 2025, 15, 6379

Synthesis of metal–organic rectangles decorated with primary amide groups for the synergistic Lewis acid and Brønsted base heterogeneous catalysis

Alokananda Chanda and Sanjay K. Mandal *

This work reports the one-pot self-assembly of two Zn/Cd-based molecular rectangles (**1** and **2**, respectively) with a new ligand containing a primary amide group, 2-(*tert*-butyl(pyridin-2-ylmethyl) amino) acetamide (bpaa), under ambient conditions. Based on the single crystal X-ray structures of **1** and **2**, molecular rectangles have an average dimension of ~7.9 × ~7.2 Å. Both **1** and **2** are thermally stable up to 275 °C and their chemical resistance towards solvents (methanol and water), and acidic and basic environments (pH: 5, 7.4 and 9) monitored by powder X-ray diffraction is remarkable. The synergistic presence of the Lewis acidic metal centers and the Brønsted basic nature of the free –NH_2 groups in **1** and **2** has powered these very efficient (catalyst: 1.5 mol%; time: 3 h) and recyclable catalysts for making multipurpose coumarin-3-carboxylic acids *via* the Knoevenagel-intramolecular tandem cyclization reaction of Meldrum's acid with salicylaldehyde under green conditions (solvent: methanol; temperature: 25 °C). In addition to a broad substrate scope, the mechanistic pathway has been supported by an experimental proof where the interaction of free –NH_2 groups in **1** and **2** with Meldrum's acid and that of the Lewis acid metal centers with salicylaldehyde is evident from the fluorescence quenching of the catalysts that is not observed for other catalysts not having such groups. Our findings provide an encouraging strategy for utilizing such combination of active sites for other multi-component organic transformations.

Received 1st July 2025,
Accepted 31st July 2025

DOI: 10.1039/d5cy00798d

rsc.li/catalysis

Introduction

The utility of metal–organic hybrid materials as heterogeneous catalysts lies in the exploration of Lewis acid metal centers and/or Lewis and Brønsted basic sites, such as an uncoordinated pyridyl group, amine group (attached to an aromatic ring or from a coordinated primary amide moiety), *etc.*, in the organic parts.[1–10] A judicious incorporation of both these functionalities in a catalyst can facilitate lowering of the reaction activation energy to a significant extent by simultaneously activating both reactants in the multi-component organic transformations, thereby enhancing the catalytic reaction. In such reactions, the Lewis acid center activates the electrophilic substrate and the Brønsted basic sites can generate suitable nucleophiles *in situ* to facilitate efficient nucleophilic attack. Until now, complicated multistep processes, such as post synthetic modification (PSM) or post synthetic exchange (PSE), have been normally adopted to make such functionalized metal–organic hybrid catalysts.[1,3] Thus, their synthesis *via* the self-assembly of components in a single-pot under ambient conditions is highly preferred.

Considering the limited literature on such catalysts that have been used in the multi-component organic transformations, an ideal challenge can be the synthesis of coumarin-3-carboxylic acids (C-3-CAs) and their derivatives, which have a huge importance in agrochemical, food, perfume, pharmaceutical and cosmetics industries.[11] Specifically, the biological properties of coumarin derivatives, such as anti-inflammatory, antiviral, antifungal, antidiabetic, antibiotic, antioxidant, anticoagulant, antitumor, and anti-HIV-1 properties, have been widely explored in the pharmaceutical industry (Scheme S1, SI).[12–16] For example, warfarin, which has a coumarin core, is an important anticoagulant used to prevent and treat venous thrombosis and thromboembolic events, as well as conditions such as myocardial infarction and atrial fibrillation. Likewise, several coumarin derivatives are known for the treatment of Alzheimer's disease.[4] Furthermore, C-3-CAs have also been commonly utilized as detectors for hydroxyl radicals in aqueous media,[17] triplet oxygen sensitizers,[18] and as

Department of Chemical Sciences, Indian Institute of Science Education and Research Mohali, Sector 81, Manauli PO, S.A.S. Nagar, Mohali, Punjab 140306, India. E-mail: sanjaymandal@iisermohali.ac.in

fluorophores.[19] These derivatives are also known to be explored in the field of neurology for the treatment of various neurological disorders.[20] Additionally, its ester and amide derivatives also exhibit biological activities.[4]

However, several methods in the literature for the synthesis of coumarin-3-carboxylic acids employed harsh conditions like high temperature, high boiling solvents, high reaction time, high catalyst loadings, and dangerous chemicals such as concentrated H_2SO_4.[22–31] For instance, a two-step method involving the Knoevenagel condensation of 2-methoxybenzaldehydes with Meldrum's acid in DMF followed by cyclization in presence of H_2SO_4 was introduced by Armstrong and his coworkers.[22] The same reaction with excess ZnO at 80 °C has also been executed but in the solid phase.[23] In the following years, one-pot methods utilizing *ortho*-hydroxyarylaldehyde and Meldrum's acid have come into the scene; however, these required either dangerous reagents (solid catalysts, ammonium acetate, sodium azide, piperidinium acetate, *etc.*), harsh conditions (microwave irradiation, reflux) or complicated work-up processes.[24–28] Some groups have reported that the thermal activation in an aqueous medium can effectively replace the need for a catalyst.[29,30] A solid-phase synthetic route using ethylmalonate was also established, but it required pyridine as a solvent.[31]

Thus, renewed effort was warranted to identify suitable metal–organic hybrid compounds for catalysing the Knoevenagel-intramolecular tandem cyclization reaction of Meldrum's acid with various salicylaldehydes to synthesize C-3-CAs under mild conditions. As shown in Scheme 1 (top), our group has been rigorously involved in the synthesis of coumarin-3-carboxylic acids, exploring metal–organic bifunctional catalysts for the past few years.[4,5] The first such example, a ladder-like polymer, $\{[Cd_2(2\text{-BPXG})(Fum)_2(H_2O)_2]\cdot 2H_2O\}_n$ (where, 2-BPXG = 2,2′-((1,4phenylenebis(methylene))bis((pyridin-2-ylmethyl) azanediyl)) diacetamide and Fum = fumarate), contain metal centers and free NH_2 (from a coordinated primary amide moiety) groups as Lewis acid and Brønsted basic sites, respectively (Scheme 1i, top).[4] On the other hand, in $\{[Cd_2(4\text{-tpom})_2(oxdz)_2(H_2O)_2]\cdot 4H_2O\}_n$ (where 4-tpom = (tetrakis(4-pyridyloxymethylene)methane) and $oxdz^{2-}$ = (4,4′-(1,3,4-oxadiazole-2,5-diyl)-dibenzoate)), with a 2D architecture, the uncoordinated pyridyl groups act as the Brønsted basic sites, whereas the metal centers act as Lewis acid sites (Scheme 1ii, top).[5] The synergistic activation of both the substrates (salicylaldehyde and Meldrum's acid) by

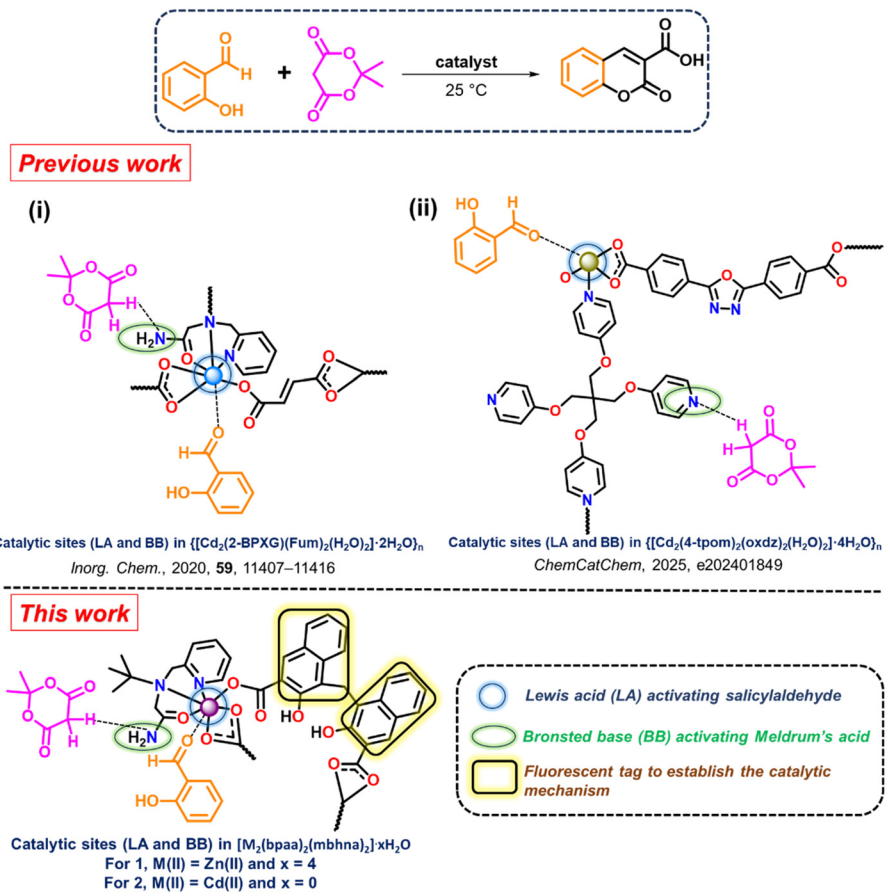

Scheme 1 Previous work (i and ii, top) and this work (bottom) with respect to the functional moieties in the metal–organic bifunctional (Lewis acid and Brønsted base) metal–organic catalysts for the synthesis of coumarin-3-carboxylic acid at 25 °C.

these bifunctional catalysts resulted in the successful generation of C-3-CAs in good yields. However, no in-depth mechanistic study could be carried out to understand the roles of such dual active sites in the catalysts.

In order to provide an understanding of the interactions of both the Lewis acid and Brønsted base in the catalysts with two substrates used in the formation of coumarin-3-carboxylic acids, we desired for the judicious incorporation of a fluorescent tag preferably in the carboxylate linker to monitor the presumed interactions *via* fluorescence spectroscopy. Furthermore, with a preference to have the free NH_2 group (from a coordinated primary amide moiety) as the Brønsted basic site, a discrete heterogeneous catalyst for such organic transformation was aimed as only polymeric metal–organic heterogeneous catalysts were reported until now. In view of this, we utilized our effort in the past 15 years with several tridentate capping ligands that led to the discovery of diverse metal–organic hybrid materials ranging from molecular rectangles/squares to 1D-3D coordination polymers (CPs)/networks.[32–34] Among the factors that govern the formation of either CPs or molecular rectangles/squares, the flexibility and angularity of a dicarboxylate that imposes synthetic challenges has been most crucial.[35] In particular, a combination of the most explored tridentate capping ligand, bpta (*N*,*N*′-bis(2-methylpyridyl)-*t*-butylamine), and Zn(II)/Cd(II) provided 1D CPs for flexible dicarboxylates like $mbhna^{2-}$ (4,4′-methylene-bis(3-hydroxy-2-naphthalene carboxylate)),[33] but it provided molecular squares for 4,4′-(dimethylsilanediyl)bis-benzoate acid and 4,4′-oxybis-benzoate.[34] Utilizing such knowledge, a new tridentate ancillary ligand grafted with a primary amide group replacing a pyridyl group in bpta, 2-(*tert*-butyl(pyridin-2-ylmethyl) amino) acetamide (bpaa), was designed with a target to obtain molecular rectangles of the fluorescent tag bearing dicarboxylate ($mbhna^{2-}$) as shown in Scheme 1, bottom.

Gratifyingly, we were able to synthesize and isolate under ambient conditions two molecular rectangles having a formula, $[M_2(bpaa)_2(mbhna)_2]\cdot xH_2O$, where M(II) = Zn(II) and x = 4 for **1** and M(II) = Cd(II) and x = 0 for **2**, in high yields. The molecular structures of **1** and **2** determined by single crystal X-ray diffraction study confirmed their isostructural nature. For the change from bpta to bpaa, the formation of **1** and **2** was possible due to the versatility of $mbhna^{2-}$ with monodentate and chelated bidentate binding modes on each end, breaking the trend for the dicarboxylates mentioned above. Amazingly, rectangles **1** and **2** are very stable toward thermal and chemical treatments (different solvents and a range of pH), providing an opportunity to use them in various applications. Having both the Lewis acidic metal centers and Brønsted basic nature of the free NH_2 groups, rare in a single catalyst, both **1** and **2** have been found to be very efficient (only 1.5 mol%) and recyclable heterogeneous catalysts for the Knoevenagel-intramolecular tandem cyclization reaction of Meldrum's acid with various salicylaldehydes to synthesize coumarin-3-caboxylic acids and their derivatives in methanol at 25 °C. The use of a greener solvent like methanol, no external heat source, and much less time are the notable features of this work. Furthermore, having no coordinated water molecules in **1** and **2**, there is no difference between the as-synthesized *vs.* activated **1** and **2** for catalysis. To the best of our knowledge, these are the first examples of discrete heterogeneous metal–organic catalysts for such organic transformation.

Experimental section

The materials and characterization methods section is described in the SI. $\{[Zn(mbhna)(bpta)]\}_n$ (**3**) and $\{[Cd(mbhna)(bpta)(CH_3OH)]\}_n$ (**4**) were made following the literature methods.[33] The spectroscopic (FTIR) data and powder X-ray diffractograms matched well with the reported ones confirming their identity (Fig. S1, SI).

Synthesis of 2-(*tert*-butyl(pyridin-2-ylmethyl)amino)acetamide (bpaa)

The synthesis of bpaa involves two steps, where 2-methyl-*N*-(pyridin-2-ylmethyl)propan-2-amine (2-mppa) is an intermediate.

Step 1: in a dropwise manner, *t*-butyl amine (0.63 mL, 6 mmol) was added to 2-pyridinecarboxaldehyde (0.47 mL, 5 mmol) in 7 mL of dry methanol placed in a 50 mL two-neck round-bottomed flask (RBF) at room temperature. Upon stirring the mixture for 4 h, a clear yellow solution was obtained. An excess of sodium borohydride (350 mg) was then added to it in portions at 0 °C with constant stirring. Further stirring of the mixture was continued for another 6 h. The isolation of the desired product involved an extraction with chloroform and water, followed by drying with anhydrous Na_2SO_4 and removal of chloroform under vacuum. A brown oily product was obtained. Yield: 584 mg (71%). ^{1}H NMR (400 MHz, $CDCl_3$, δ ppm): δ 8.52 (1H, d), 7.60 (1H, m), 7.32 (1H, d), 7.12 (1H, m), 3.87 (2H, s), 1.10 (9H, s). Selected FT-IR peaks (KBr, cm^{-1}): 3440 (b), 2917 (w) 1640 (s), 1216 (w), 759 (s).

Step 2: in a 50 mL RBF, 2-mppa (400 mg, 2.43 mmol) in 15 mL of dry acetonitrile and solid K_2CO_3 (1.8 g, 13 mmol) were taken under a N_2 atmosphere and stirred for 1 h. Then, 2-bromoacetamide (362 mg, 2.62 mmol) in 15 mL of dry acetonitrile was added to it in a dropwise manner. Upon refluxing the mixture for 24 h, it was brought to room temperature. The liquid phase was collected by filtering out the solid residue that was washed with 2 × 10 mL of methanol. Upon evaporation of solvents, a solid residue was obtained. The solid residue was redissolved in dry methanol to filter off any solid and then methanol was evaporated under vacuum to isolate an oily substance. Finally, 10 mL of $CHCl_3$ was added to the oily substance at 0 °C to obtain a dark brown semi-solid following the filtration/evaporation of the solvent. Yield: 300 mg (56%) with respect to 2-mppa. ^{1}H NMR (400 MHz, $CDCl_3$, δ ppm): 8.44 (1H, d), 7.52 (1H, m), 7.24 (1H, d), 7.05 (1H, m), 3.78 (2H, s), 3.20 (2H, s), 1.10 (9H, s). ^{13}C NMR (400 MHz, $CDCl_3$, δ ppm): 26.79, 54.66, 55.74,

57.22, 122.07122.78, 136.60, 149.23, 160.69, 177.02. Selected FT-IR peaks (KBr, cm^{-1}): 3444 (b), 2963 (w) 2917 (w), 1644 (s), 1408 (w), 1216 (s), 771 (s), 673 (w).

Synthesis of $[Zn_2(bpaa)_2(mbhna)_2]\cdot 4H_2O$ (1)

A mixture of 2 mL methanolic solution of bpaa (22 mg, 0.1 mmol) and 1 mL aqueous solution of $Zn(OAc)_2\cdot 2H_2O$ (22 mg, 0.1 mmol) was prepared in a 10 mL RBF and stirred for 15 min to obtain a clear brown solution. Upon addition of an aqueous solution (1 mL) of Na_2mbhna (39 mg, 0.1 mmol) to this brown clear solution, a white precipitate appeared instantly at 25 °C. The amount of the precipitate gradually increased with time and the stirring was stopped after 12 h. The mixture was filtered, washed with water and methanol several times (3 × 2 mL), and then air-dried to isolate the product. Yield: 55 mg (77.5%), based on the metal salt. Anal. calcd. for $C_{70}H_{74}N_6O_{18}Zn_2$ (MW 1418.15): % C, 59.29; % H, 5.26; % N, 5.93. Found: % C, 59.11; % H, 5.23; % N, 5.33. Selected FTIR peaks (KBr, cm^{-1}): 3428 (br), 1673 (s), 1644 (s), 1457 (s), 1392 (s), 1351 (s), (s), 869 (w) and 759 (s).

Synthesis of $[Cd_2(bpaa)_2(mbhna)_2]$ (2)

A mixture of 2 mL methanolic solution of bpaa (22 mg, 0.1 mmol) and 1 mL aqueous solution of $Cd(OAc)_2\cdot 2H_2O$ (27 mg, 0.1 mmol) was prepared in a 10 mL RBF and stirred for 15 min to obtain a clear brown solution. Upon addition of an aqueous solution (1 mL) of Na_2mbhna (39 mg, 0.1 mmol) to this brown clear solution, a white precipitate appeared instantly at 25 °C. The amount of the precipitate gradually increased with time and the stirring was stopped after 12 h. The mixture was filtered, washed with water and methanol several times (3 × 2 mL), and then air-dried to isolate the product. Yield: 58 mg (80.5%), based on the metal salt. Anal. calcd. for $C_{70}H_{66}Cd_2N_6O_{14}$ (MW 1440.16): % C, 58.38; % H, 4.62; % N, 5.84. Found: % C, 58.22; % H, 4.89; % N, 5.82. Selected FTIR peaks (KBr, cm^{-1}): 3460 (br), 1673 (s), 1636 (s), 1555 (s), 1457 (s), 1398 (s), 1351 (s), 861 (w) and 767 (s).

General procedure for the Knoevenagel-intramolecular tandem cyclization reaction

Typically, a mixture of salicylaldehyde (0.1 mmol), Meldrum's acid (0.15 mmol), and 1.5 mol% of activated **1** or **2** was stirred for the required period of time in 1 mL of solvent, in a 5 mL round-bottom flask at 25–28 °C. The reaction mixture was centrifuged to collect the crude product that was redissolved in DMSO-d_6 for NMR spectroscopy. The C-3-CAs were purified by the recrystallization method using ethanol.

Recycling of the catalysts

For the Knoevenagel-intramolecular tandem cyclization reaction, the solid catalyst was recovered from the reaction mixture by the centrifugation technique. Then, the catalyst was rinsed three times with methanol. Upon drying the recovered catalyst under vacuum for 6 h at 100 °C, it was utilized in the subsequent catalysis cycle.

Results and discussion

Synthesis and structural analysis

The bpaa ligand was synthesized in a two-step process with an overall yield of 40% (Scheme 2a). In the first step, a Schiff base condensation reaction occurs between *tert*-butyl amine and 2-pyridine carboxaldehyde (in a 1 : 1 ratio) in dry CH_3OH followed by the reduction of the intermediate imine by excess

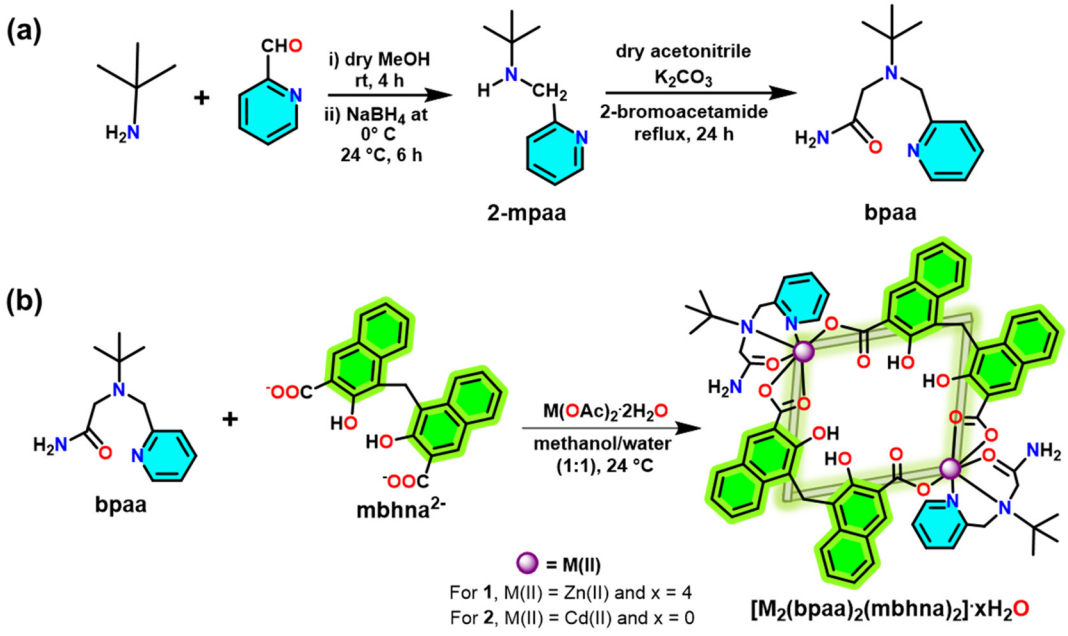

Scheme 2 Synthesis of (a) bpaa, and (b) molecular rectangles of **1** and **2**.

sodium borohydride. In the second step, a nucleophilic substitution reaction (S_N2) occurs on the reduced Schiff base with 2-bromoacetamide in dry CH_3CN with K_2CO_3 as a base. The FTIR and ^1H NMR spectrum of the reduced Schiff base intermediate and the $^1H/^{13}C$ NMR spectra of bpaa are reported in Fig. S2–S5, SI. The molecular rectangles **1** and **2** were obtained from a one-pot self-assembly of $M(OAc)_2{\cdot}2H_2O$, bpaa and $mbhna^{2-}$ (in a 1 : 1 : 1 ratio) by stirring at 24 °C for 12 h in a methanol–water mixture (Scheme 2b). After washing the isolated product several times with water and methanol, it was air-dried.

Colourless crystals of **1** and **2** that were found to be ideal for SCXRD analysis were grown by direct layering of the components in a methanol–water mixture. The single crystal structure analysis reveals that both **1** and **2** crystallize in the triclinic $P\bar{1}$ space group, confirming their isostructural nature (see the CIF files for further details). In each case, two independent molecules (**A** and **B**) are found in the asymmetric units, each of which has one bpaa ligand, one metal ion and one dicarboxylate. One of the molecules (A) of **1** and **2** have been depicted in Fig. 1a and b, respectively. The fully labelled ORTEP diagrams of **1** and **2** are shown in Fig. S6 and S7, SI, respectively. The corresponding space fill models of **1** and **2** shown in Fig. 1c and d clearly show the oxygen-rich environment inside the pores. In the molecular rectangles (dimensions - **1**: 7.897 × 7.091 Å and 7.917 × 7.159 Å; **2**: 8 × 7.375 Å and 7.941 × 7.381 Å for **A** and **B** molecules, respectively), each metal center is hexacoordinated. Each metal center is connected to two nitrogen atoms and one oxygen atom of the bpaa ligand and three oxygen atoms of two different dicarboxylates giving rise to a distorted octahedral geometry. The dicarboxylate binds to the metal centers in a monodentate fashion with one end and in a bidentate chelating fashion with the other end. Due to such binding modes of $mbhna^{2-}$ in **1** and **2**, the angles around the CH_2 group are 94.84° and 90.74°, respectively. In the 1D CPs of the bpta analogs of **1** and **2**, the corresponding angles of 113.36–118.48° around the CH_2 group only confirm the flexibility of $mbhna^{2-}$.[33] On the other hand, the molecular squares constructed with 4,4′-(dimethylsilanediyl)bis-benzoate and 4,4′-oxybis-benzoate are strikingly different, where the dicarboxylates bind in a bis(monodentate) fashion leaving space for a coordinated water molecule on each metal center.[34] This difference can be understood based on the angularity in 4,4′-(dimethylsilanediyl)bis-benzoate (angles of 106.06–106.68° around the Si atom) and 4,4′-oxybis-benzoate (angles of 116.14–117.10° around the O atom). The average $Zn–O_{carb}$ bond lengths (**1**: 1.966–2.502 Å; **2**: 2.177–2.532 Å) and $Zn–O_{amide}$ bond lengths (**1**: 2.101–2.103 Å; **2**: 2.295–2.298 Å) corroborate well with those for the compounds having similar ligands.[33,36–38]

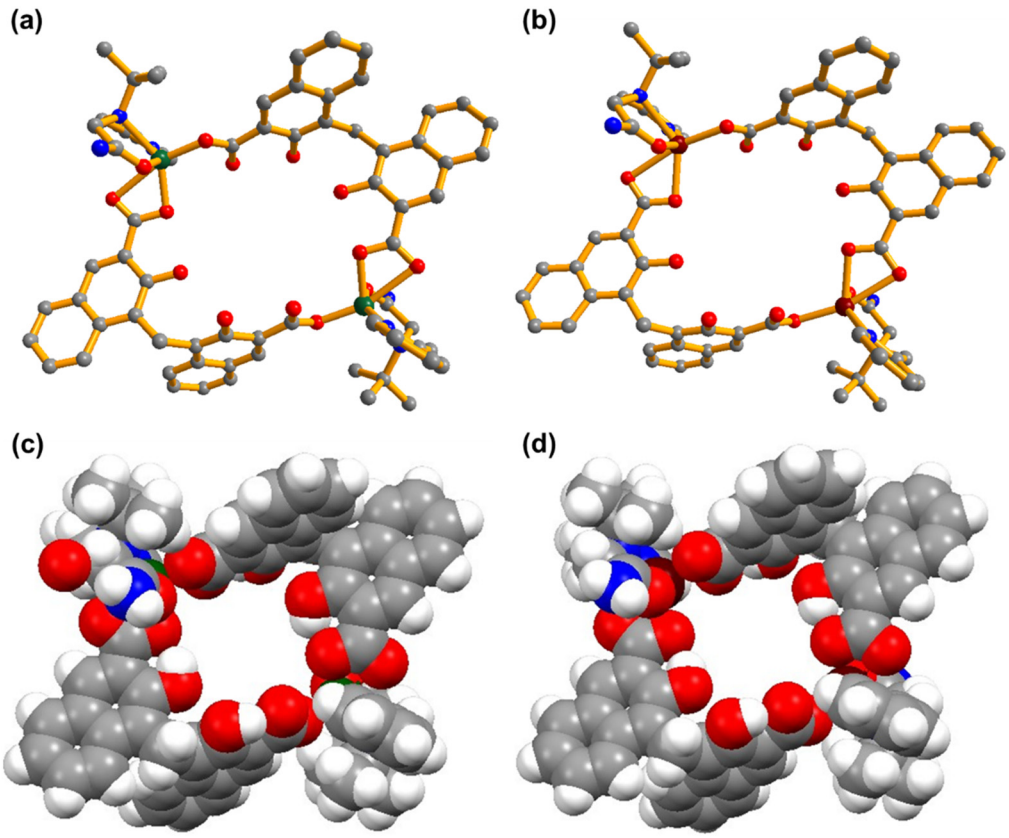

Fig. 1 (a and b) single crystal structures of **1** and **2**, respectively. Hydrogen atoms are not shown for clarity. (c and d) Space-fill models of **1** and **2**, respectively. Only **A** molecules for each are shown.

In the molecular rectangles, the alignment of bpaa and $mbhna^{2-}$ is such that four OH groups and two uncoordinated carbonyl O atoms of the dicarboxylate point toward the inner side of the cavity, while two NH_2 groups point outside the cavity. However, each one-half of these atoms/groups are below and above the plane defined by the metal centers and the CH_2 groups of $mbhna^{2-}$. Furthermore, moderate π···π interactions between the adjacent molecular rectangles of **A** (π···π distance: 3.682 Å in **1** and 3.861 Å in **2**) due to the face–face stacking of the naphthalene rings of the dicarboxylates, thereby generating a supramolecular assembly (Fig. S8, SI). Notably, such supramolecular interaction is absent between the molecular rectangles of **B** in both **1** and **2**.

In the FTIR spectra of **1** and **2** (Fig. 2a and S9, SI), the appearance of a strong peak at 1673 cm^{-1} confirms the presence of coordinated –C(═O)NH_2 groups.[36,37] The strong peaks at 1644/1392 cm^{-1} and 1575/1351 cm^{-1} for **1** and at 1636/1396 cm^{-1} and 1555/1351 cm^{-1} for **2** correspond to the asymmetric and symmetric stretching frequencies of carboxylate groups of $mbhna^{2-}$, respectively. The observed differences between the two stretching frequencies of 240–252 cm^{-1} and 204–224 cm^{-1} indicate monodentate and bidentate chelated binding modes of the dicarboxylate to the metal centers respectively, which is corroborated with their single crystal structures discussed above.[39] The peaks of moderate intensity, at 754–767 cm^{-1}, are due to the C═N stretches of pyridyl groups.

Additionally, their formula was confirmed by the CHN analysis and the thermogravimetric (TG) profiles obtained between 30 and 500 °C under a dinitrogen atmosphere. The TG profiles of **1** and **2** are shown in Fig. 2b. A weight loss of around 4.3% between 30–79 °C is encountered in the TG profile of **1**, which is due to the elimination of four water molecules from the lattice sites (calculated: 5%). Beyond 79 °C, it was stable up to 277 °C. On the other hand, in the TG profile of **2**, no weight loss was observed between 30–79 °C indicating the absence of solvent molecules in the lattice sites. Like **1**, the stability of **2** is up to 277 °C. Upon further heating, both **1** and **2** undergo decomposition due to the loss of CO_2 from the dicarboxylates as indicated by the sharp weight loss. It is notable that the thermal stability of such discrete molecular rectangles is unusual.

The bulk phase purity of **1** and **2** was established by the PXRD diffractograms, where the experimental patterns matched well with the simulated patterns obtained from single crystal data (Fig. 3a and b). Their similar PXRD patterns also indicated that they are isostructural. Their chemical stability was also assessed by soaking them in different solvents (water and methanol) as well as in different pH solutions for three days (Fig. 3a and b). The PXRD diffractograms recorded after this treatment matched well with that of the as-synthesized materials, confirming the retention of their structural integrity. The chemical stability of such discrete molecular rectangles under such harsh conditions is rare. The morphological study of the as-isolated **1** and **2** by FESEM indicates that both are aggregations of very tiny particles with a size range of 70–120 nm (Fig. S10, SI).

The full range XPS spectra of **1** and **2** are shown in Fig. 4a and b, where peaks for all the component elements, C, N, O, and Zn in **1** and Cd in **2** are evident. On further deconvolution of the elemental spectra, the existence of different functional groups in the molecular rectangles was investigated (Fig. 4c–f and Fig. S11, SI). For **1**, the deconvoluted spectra of the Zn 2p orbitals showed further splitting into two components with a difference of ~23 eV between $2p_{3/2}$ and $2p_{1/2}$.[40] On the other hand, such a difference in **2** for Cd $3d_{5/2}$ and $3d_{3/2}$ was 6.7 eV.[5] The C 1s spectrum splits into three components due to C–C/C═C, C–N, and O–C═O at 284.8, 286.045, and 288.6 eV, respectively. While N 1s splits into two components: one appears at around 399 eV due to the pyridyl nitrogen atom and the other appears at around 400 eV due to the amide N atom, on the other hand, on deconvolution of the O 1s

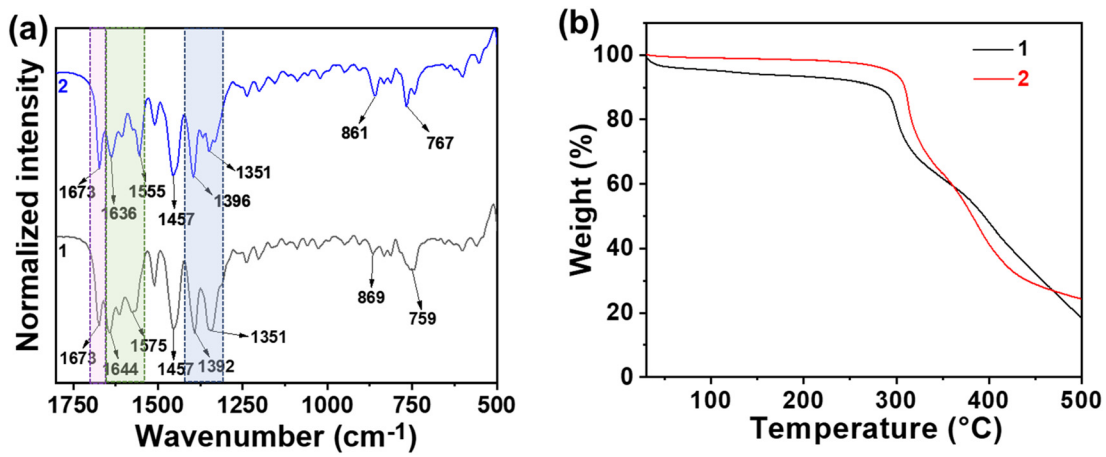

Fig. 2 (a) FTIR and (b) TGA of **1** and **2** (in (a), amide carbonyl, asymmetric and symmetric carboxylate stretches are shaded in pink, green, and blue, respectively).

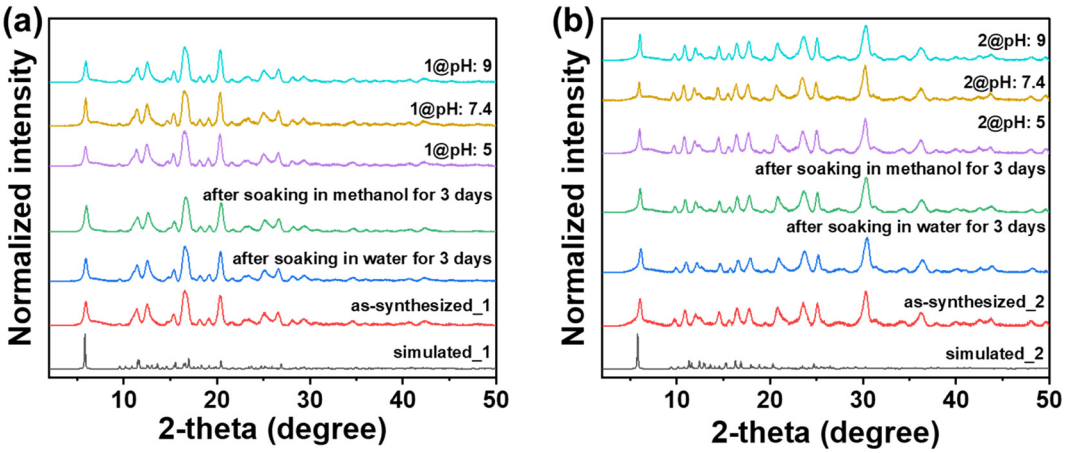

Fig. 3 (a and b) Simulated and PXRD spectra of **1** and **2**, respectively, before (as-synthesized) and after treatment in different solvents and at different pH solutions.

spectrum, it splits into two components such as C═O (531 eV) and C–O (532 eV).

Knoevenagel-intramolecular tandem cyclization reaction catalyzed by 1 and 2

Having the Lewis acidic metal centers and the free NH_2 groups of the bpaa ligand in **1** and **2**, both were utilized in the Knoevenagel-intramolecular tandem cyclization reaction of Meldrum's acid (2,2-dimethyl-1,3-dioxane-4,6-dione) with several salicylaldehydes to synthesize a number of derivatives of coumarin-3-carboxylic acids (**a–i**) (Fig. 5a). In a typical reaction, Meldrum's acid (0.15 mmol), salicylaldehyde (0.1 mmol), and activated (carried out in a vacuum oven at 100 °C for 6 h) **1**/**2** (1.5 mol%) were stirred in 1 mL of solvent at 25 °C. The first step toward optimizing the reaction conditions was screening with respect to time. Two sets of reactions were carried out in the presence of **1** and **2**, in 1 mL of methanol for 1, 2, 2.5 and 3 h (Fig. 5b). For **1**, in the initial first hour, we could achieve only 24 (±1.3)% of conversion. Therefore, the reaction time was further increased to 2 and 2.5 h to obtain 41 (±1.7) and 62 (±2.5)% of conversion, respectively. However, 99% conversion was attained after 3 h. Similarly, for **2**, the reaction was also monitored after 1, 2, 2.5 and 3 h. The corresponding conversions were found to be 32 (±1.8), 44 (±3), 76 (±4.5) and 99%, respectively (Fig. 5b).

For confirming methanol is the best solvent for this reaction, other solvents were also used under the same reaction conditions with the conversion (%) in the following order: for **1**, methanol > chloroform > ethyl acetate > acetonitrile > tetrahydrofuran; for **2**, methanol > ethyl acetate > chloroform > acetonitrile > tetrahydrofuran (Fig. 5c). It should be noted that the catalysis reactions without activation of **1** and **2** provided the same results, simplifying the process and lowering the cost. This reaction was also performed with 3 mol% of $\{[Zn(bpta)(mbhna)]\}_n$ (**3**) and $\{[Cd(bpta)(mbhna)(CH_3OH)]\}_n$ (**4**)[33] (lacking any amide group) under the optimized reaction conditions only to obtain a conversion of 48 (±2.8) and 41 (±1.4)%, respectively (Fig. 5d). Similarly, a control run without any catalyst provided only 13 (±2.1)% conversion (Fig. 5c), indicating the importance of the primary amide grafted catalysts. Furthermore, the reaction carried out with 3 mol% of $Zn(OAc)_2{\cdot}2H_2O$ or $Cd(OAc)_2{\cdot}2H_2O$ (under the same conditions but homogeneous) provided 30 (±1.4) and 26 (±1.4)% of conversion, respectively (Fig. 5d). The corresponding conversion (%) was determined by ^1H NMR spectroscopy (Fig. S12–S18, SI).

In order to establish the versatile nature of catalysts, products of various substituted salicylaldehydes (**a–i**) are reported in Scheme 3 under the optimized conditions. It is observed that both electron withdrawing (EW) and electron donating (ED) substituents result in >97% conversion of the salicylaldehyde (Fig. S19–S34, SI). Notably, a conversion of >99% for 2-hydroxy-1-naphthaldehyde into its corresponding cyclic acid (**i**) is obtained, indicating that both Lewis acidic and Brønsted basic sites present within the pores and on the surface of the catalysts are easily accessible to the substrates irrespective of their sizes. The C-3-CA (**a**) made from the reactions catalysed by **1** and **2** was isolated and recrystallized from ethanol; their $^1H/^{13}C$ NMR spectra are reported in Fig. S35–S38, SI. The substituted C-3-CAs (**b–i**) isolated from the reactions catalysed by **2** were also crystallized and characterized by $^1H/^{13}C$ NMR spectroscopy (Fig. S39–S54). For all these products (**a–i**) obtained from the reactions catalyzed by **2**, the % yield, turn over number (TON), turn over frequency (TOF), and melting point values are given in Table S1, SI. Interestingly, their isolated yields (%) shown in Scheme 3 are in good agreement with the corresponding% conversions.

The efficiency of **1** and **2** is comparable to that of $\{[Cd_2(2\text{-}BPXG)(fum)_2(H_2O)_2]{\cdot}2H_2O\}_n$ and $\{[Cd_2(4\text{-}tpom)_2\ (oxdz)_2(H_2O)_2]{\cdot}4H_2O\}_n$ reported in our previous work.[4,5] On the other hand, the catalyst loading for **1** and **2** is lower than that of CdO_**3a**.[21] The structural difference between the molecular rectangles **1** and **2** and the ladder-like polymeric architecture

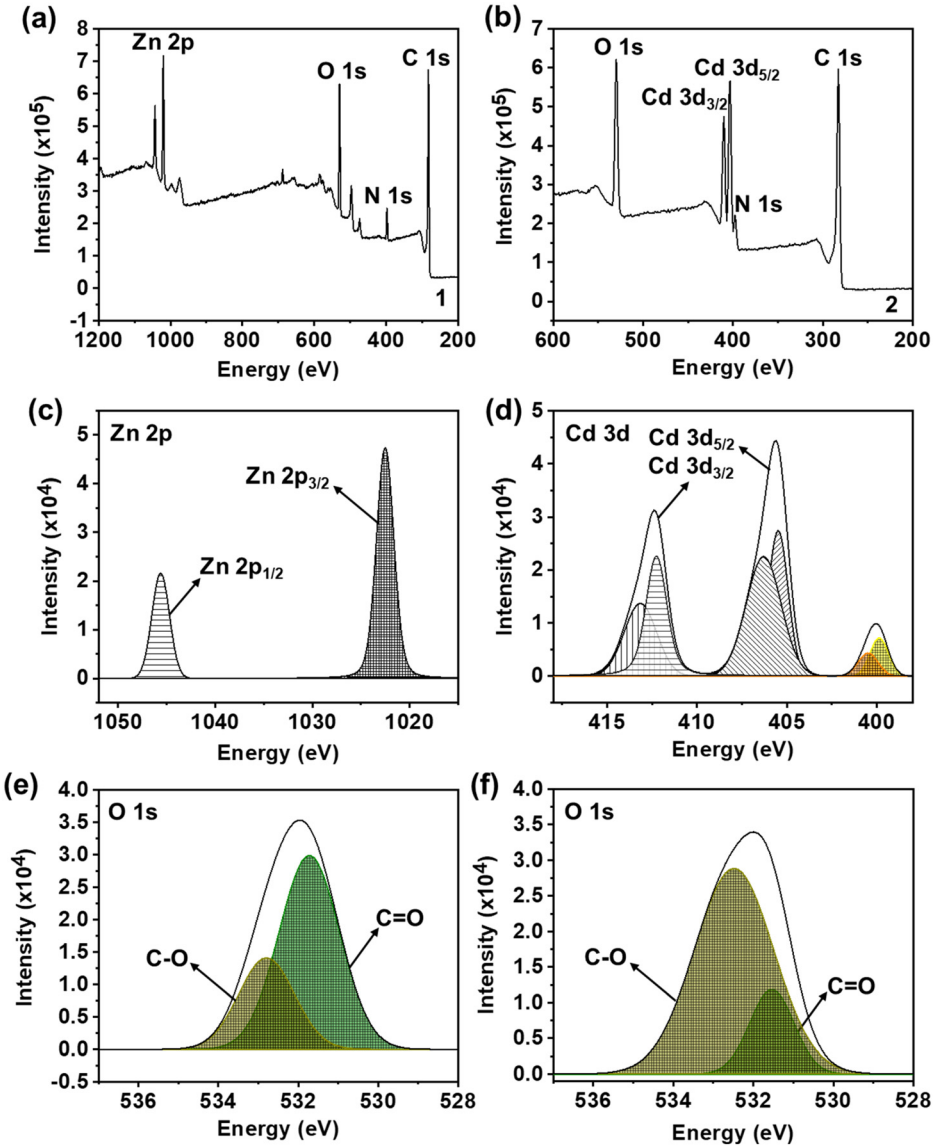

Fig. 4 (a and b) Full range XPS spectra of **1** and **2**, respectively. (c and d) Deconvoluted XPS spectra of Zn 2p and Cd 3d in **1** and **2**, respectively. (e and f) Deconvoluted XPS spectra of O 1s in **1** and **2**, respectively.

of $\{[Cd_2(2\text{-BPXG})(fum)_2(H_2O)_2]\cdot 2H_2O\}_n$ arises from the use of a tridentate and bis(tridentate) ligand with a xylylene spacer, respectively. Thus, the use of discrete molecular rectangles with an amide group as a heterogeneous catalyst is somewhat unexpected. Gratifyingly, we could pursue it due to the exceptional thermal and chemical stability of **1** and **2**. Moreover, in this study, we also have an opportunity to compare the catalytic efficiency between **1** and **2**. On the other hand, the strategy to utilise $\{[Cd_2(4\text{-tpom})_2(oxdz)_2(H_2O)_2]\cdot 4H_2O\}_n$ for the same catalysis was to have a dangling pyridyl group presented as a Brønsted base. The catalytic efficiency for the discrete molecular rectangles lies in between those of $\{[Cd_2(2\text{-BPXG})(fum)_2(H_2O)_2]\cdot 2H_2O\}_n$ and $\{[Cd_2(4\text{-tpom})_2(oxdz)_2(H_2O)_2]\cdot 4H_2O\}_n$. Such a comparative study with catalysts containing different Brønsted bases and having discrete and polymeric structures enriches the literature. Furthermore, a comparison of the efficiency of **1** and **2** with other heterogeneous catalysts is shown in Table S2, SI.

One of the reasons for choosing heterogeneous catalysts over homogeneous catalysts is the former's easy regeneration from the reaction medium. In this case, the catalysts were regenerated *via* filtration, then washed several times with methanol (3 × 1.5 mL). After activating for 6 h at 120 °C in a vacuum oven the catalysts were then made ready for the subsequent runs. The efficiency of the catalyst remained unaltered for up to three runs (Fig. 6). The unaltered PXRD patterns and FTIR spectra recorded before and after three runs of catalysis confirmed the retention of their stability (Fig. S55–S58, SI).

The heterogeneous nature of the catalysts (**1** and **2**) was examined by a control experiment where the catalyst was

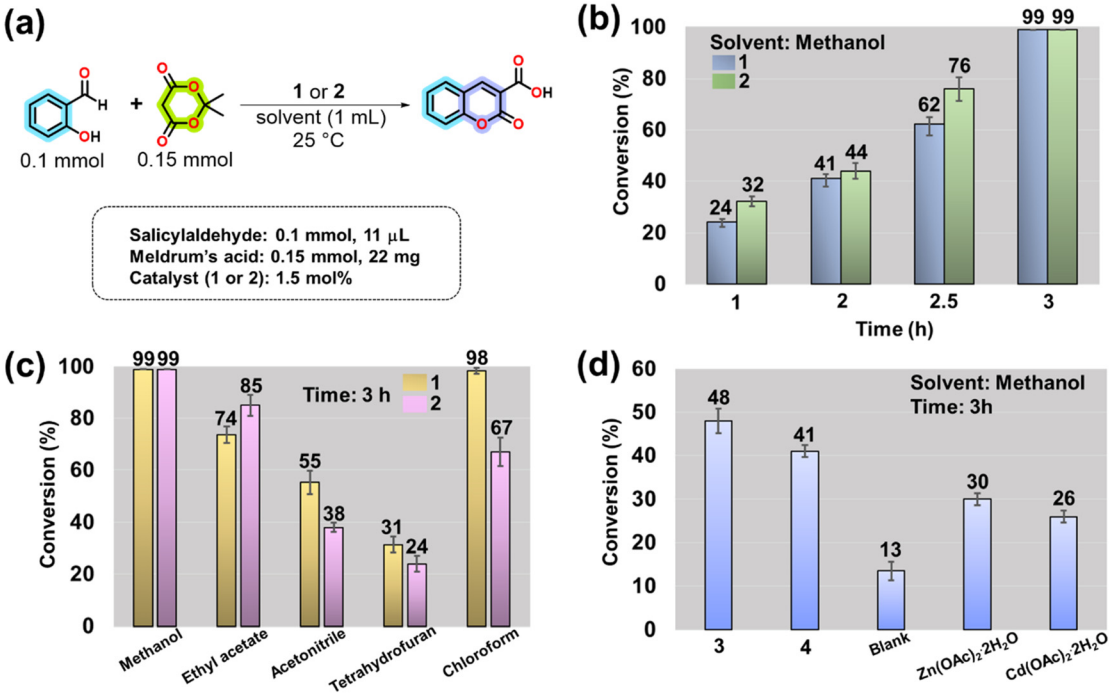

Fig. 5 (a) Schematic representation of the Knoevenagel-intramolecular tandem cyclization reaction along with the reaction conditions. (b) Bar plot depicting conversion (%) of salicylaldehyde with respect to time. (c) Bar plot depicting conversion (%) of salicylaldehyde in the presence of 1 mL of different solvents. (d) Bar plot depicting the conversion (%) of salicylaldehyde in the presence of **3** (3 mol%), **4** (3 mol%), in the absence of catalyst, and in the presence of starting metal salts (3 mol%). The numbers with error bars shown in the plots are based on three runs (for conversions of 99%, the same numbers were obtained in all three cases).

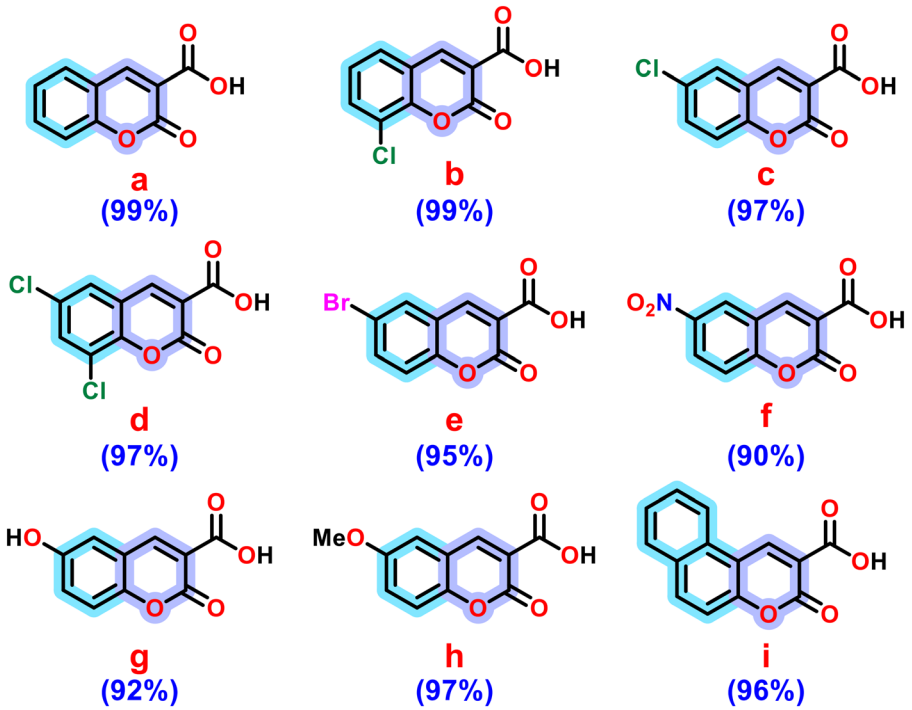

Scheme 3 Substrate scope with conditions used: derivatives of salicylaldehyde (0.1 mmol), Meldrum's acid (0.15 mmol), and **2** (1.5 mol%) at 25 °C in methanol. Numbers in parentheses are the isolated yields (%) of C-3-CAs.

removed from the respective reaction medium after stirring the reaction mixture for 1 h (Fig. S59, SI). The conversion (%) determined at this point was found to be 23% and 27%, respectively. After stirring under the same conditions but

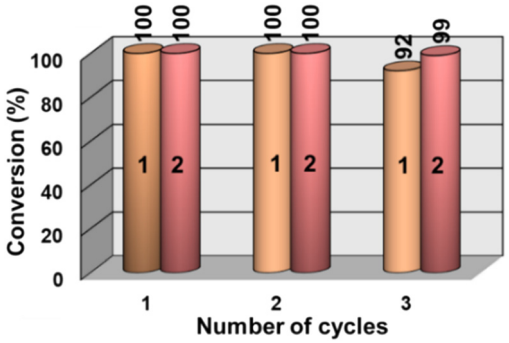

Fig. 6 Plot of conversion (%) for three consecutive cycles of the reaction catalyzed by **1** and **2**.

without the catalysts for another 2 h resulted in no significant advancement in the formation of the product. This observation confirms the role of the catalysts in the course of the reaction. The energy-dispersive X-ray (EDX) analysis of the organic supernatant showed no trace amount of metals, confirming the leach-proof nature of the catalysts (Fig. S60 and S61, SI).

Finally, Fig. 7a shows a plausible mechanism for this reaction. In the first step, the Lewis acidic metal centers in **1** and **2** activate the salicylaldehyde carbonyl group. This is followed by the deprotonation of Meldrum's acid assisted by the Brønsted basic NH_2 groups. The carbonyl oxygen of the primary amide group is coordinated to a metal center in **1** and **2**, and thus, its behaviour is somewhat different from a free $CONH_2$ moiety. With no size selectivity (demonstrated in substrate scope), we believe that the catalysis occurs on the surface of the rectangles. The choice between NH_2 *vs.* the uncoordinated oxygen in one of the two carboxylate groups of $mbhna^{2-}$ (monodentate side) can be considered with the fact that the latter may destabilize the structure due to protonation (forming a carboxylic acid group). For providing support to the mechanism, the interaction of salicylaldehyde and Meldrum's acid with **2** was investigated through two separate fluorescence titration experiments, where 60 μL of 2 mM solution of salicylaldehyde or Meldrum's acid was added incrementally to a homogeneous suspension of 2 mg of finely ground **2** in 2 mL of methanol. As shown in Fig. 7b and c, **2** exhibits fluorescence quenching at 554 nm (λ_{ex} = 380 nm) in the presence of salicylaldehyde (25%) and Meldrum's acid (52%). This synergistic activation increases the electrophilicity of the carbonyl carbon as well as the nucleophilic character of Meldrum's acid, facilitating easy nucleophilic attack by the deprotonated Meldrum's acid. Expectedly, similar experiments with $\{[Cd(bpta)(mbhna)(CH_3OH)]\}_n$ (**4**) resulted in 3% (for salicylaldehyde) and negligible (for Meldrum's acid) quenching (Fig. S62, SI), confirming further the role of the $CONH_2$ group in such reactions. This C–C bond forming step loses a water molecule generating the C=C bond. The second last step involves intramolecular tandem cyclization causing elimination of an acetone molecule. At the final step, protonation of the intermediate gives coumarin-3-carboxylic acid as the desired product.

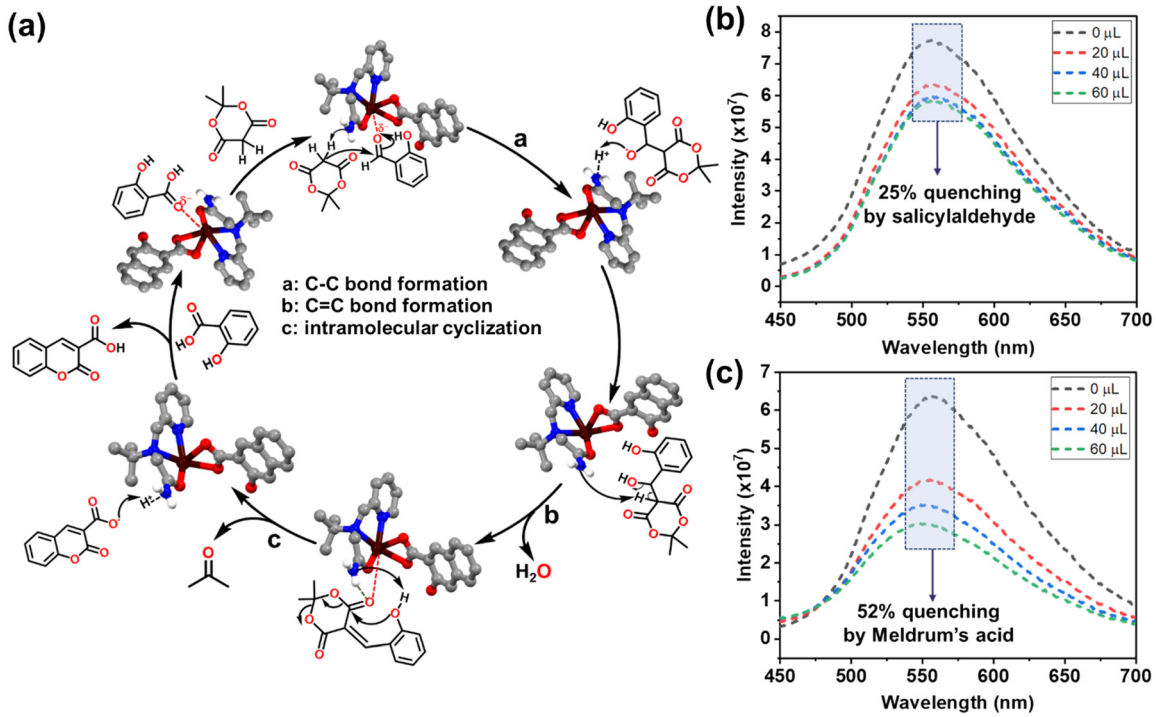

Fig. 7 (a) Plausible mechanism for the Knoevenagel-intramolecular tandem cyclization reaction. (b and c) Fluorescence titration plots of homogeneous dispersions of **2** in methanol with 2 mM solution of salicylaldehyde and Meldrum's acid, respectively.

Conclusions

In this work, the synthesis and structural features of two Zn/Cd-based molecular rectangles containing a new capping ligand with a primary amide group have been reported. Interestingly, the free NH_2 groups remain outside the cavities and are easily accessible to activate substrates along with the Lewis acidic metal centers in an organic transformation such as the Knoevenagel-intramolecular tandem cyclization reaction of Meldrum's acid with salicylaldehyde to generate coumarin-3-carboxylic acid following a green synthetic route. Notably, both the catalysts showed excellent performance with a variety of salicylaldehydes (both EW and ED groups) under the optimized conditions. The mechanistic insights of this reaction were demonstrated through (i) the fluorescence titration experiments and (ii) a comparison with polymeric analogs of **1** and **2** that contained no amide group. Owing to the interesting structural features, these molecular rectangles can also be explored as heterogeneous catalysts in many other organic transformations. Their luminescence properties are being explored in our current effort.

Conflicts of interest

There are no conflicts to declare.

Data availability

Supplementary information is available: Materials and physical methods, structural analysis and crystallographic table for **1–2**, NMR. See DOI: **https://doi.org/10.1039/D5CY00798D**.

CCDC 2426224–2426225 contains the supplementary crystallographic data for this paper.[41,42]

Data for this work is presented in this manuscript along with the SI file.

Acknowledgements

A. C. is grateful to the Ministry of Education, India, for a research fellowship. S. K. M. thanks IISER Mohali for funding and the availability of the central and departmental facilities.

References

1 A. Bavykina, N. Kolobov, I. S. Khan, J. A. Bau, A. Ramirez and J. Gascon, *Chem. Rev.*, 2020, **120**, 8468–8535.
2 L. Zhu, X.-Q. Liu, H.-L. Jiang and L.-B. Sun, *Chem. Rev.*, 2017, **117**, 8129–8176.
3 A. Corma, H. García and F. X. Llabrés i Xamena, *Chem. Rev.*, 2010, **110**, 4606–4655.
4 D. Markad, S. Khullar and S. K. Mandal, *Inorg. Chem.*, 2020, **59**, 11407–11416.
5 A. Chanda and S. K. Mandal, *ChemCatChem*, 2025, e202401849.
6 A. Dhakshinamoorthy, Z. Li and H. Garcia, *Chem. Soc. Rev.*, 2018, **47**, 8134–8172.
7 D. Yang and B. C. Gates, *ACS Catal.*, 2019, **9**, 1779–1798.
8 G.-Q. Huang, J. Chen, Y.-L. Huang, K. Wu, D. Luo, J.-K. Jin, J. Zheng, S.-H. Xu and W. Lu, *Inorg. Chem.*, 2022, **61**, 8339–8348.
9 H. Tian, S. Liu, Z. Zhang, T. Dang, Y. Lu and S. Liu, *ACS Sustainable Chem. Eng.*, 2021, **9**, 4660–4667.
10 H. Chen, L. Fan, T. Hu and X. Zhang, *Inorg. Chem.*, 2021, **60**, 7276–7283.
11 R. O'Kennedy and R. D. Thornes, *Coumarins: Biology, Applications and Mode of Action*, John Wiley and Sons, Chichester, 1997.
12 S. Emami and S. Dadashpour, *Eur. J. Med. Chem.*, 2015, **102**, 611–630.
13 U. Salar, K. M. Khan, M. I. Fakhri, S. Hussain, S. Tauseef, S. Ameer, A. Wadood, H. Khan and S. Perveen, *Med. Chem.*, 2018, **14**, 86–101.
14 X.-M. Peng, G. L. V. Damu and C. He Zhou, *Curr. Pharm. Des.*, 2013, **19**, 3884–3930.
15 K. M. Khan, Z. S. Saify, M. Z. Khan, Zia-Ullah, M. I. Choudhary, Atta-ur-Rahman, S. Perveen, Z. H. Chohan and C. T. Supuran, *J. Enzyme Inhib. Med. Chem.*, 2004, **19**, 373–379.
16 K. C. Fylaktakidou, D. J. Hadjipavlou-Litina, K. E. Litinas and D. N. Nicolaides, *Curr. Pharm. Des.*, 2004, **10**, 3813–3833.
17 Y. Manevich, K. D. Held and J. E. Biaglow, *Radiat. Res.*, 1997, **148**, 580–591.
18 D. P. Specht, P. A. Martic and S. Farid, *Tetrahedron*, 1982, **38**, 1203–1211.
19 E. Peroni, G. Caminati, P. Baglioni, F. Nuti, M. Chelli and A. M. Papini, *Bioorg. Med. Chem. Lett.*, 2002, **12**, 1731–1734.
20 M. W. Irvine, B. M. Costa, A. Volianskis, G. Fang, G. Ceolin, G. L. Collingridge, D. T. Monaghan and D. E. Jane, *Neurochem. Int.*, 2012, **61**, 593–600.
21 R. Kaur and S. K. Mandal, *ACS Appl. Nano Mater.*, 2024, **7**, 5169–5179.
22 V. Armstrong, O. Soto, J. A. Valderrama and R. Tapia, *Synth. Commun.*, 1988, **18**, 717–725.
23 F. Rouessac and A. Leclerc, *Synth. Commun.*, 1993, **23**, 2709–2715.
24 D. Sharma, S. Kumar and J. K. Makrandi, *Chem. Sci. Trans.*, 2013, **2**, 403–406.
25 B. P. Bandgar, L. S. Uppalla and D. S. Kurule, *Green Chem.*, 1999, **1**, 243–245.
26 J. L. Scott and C. L. Raston, *Green Chem.*, 2000, **2**, 245–247.
27 G. Brahmachari, *ACS Sustainable Chem. Eng.*, 2015, **3**, 2350–2358.
28 A. Song, X. Wang and K. S. Lam, *Tetrahedron Lett.*, 2003, **44**, 1755–1758.
29 M. N. Deshmukh, R. Burud, C. Baldino, P. C. M. Chan and J. Liu, *Synth. Commun.*, 2003, **33**, 3299–3303.
30 R. Maggi, F. Bigi, S. Carloni, A. Mazzacani and G. Sartori, *Green Chem.*, 2001, **3**, 173–174.
31 B. T. Watson and G. E. Christiansen, *Tetrahedron Lett.*, 1998, **39**, 6087–6090.
32 S. Khullar, V. Gupta and S. K. Mandal, *CrystEngComm*, 2014, **16**, 5705–5715.

33 A. Chanda, S. Khullar and S. K. Mandal, *Eur. J. Inorg. Chem.*, 2021, 2595–2605.
34 V. Gupta and S. K. Mandal, *Dalton Trans.*, 2018, **47**, 9742–9754.
35 A. Gogia, H. Bhambri and S. K. Mandal, *J. Mater. Chem. A*, 2024, **12**, 6476–6487.
36 D. Markad and S. K. Mandal, *ACS Catal.*, 2019, **9**, 3165–3173.
37 D. Markad, S. Khullar and S. K. Mandal, *Inorg. Chem.*, 2019, **58**, 12547–12554.
38 G. Chakraborty, P. Das and S. K. Mandal, *Chem. – Asian J.*, 2019, **14**, 3712–3720.
39 K. Nakamoto, *Infrared Spectra of Inorganic and Coordination Compounds, Part B*, John Wiley & Sons, New York, 5th edn, 1997.
40 G. Qin, G. Y. Kong, T. Gan and Y. Ni, *Inorg. Chem.*, 2022, **61**, 8966–8975.
41 A. Chanda and S. K. Mandal, CCDC 2426224: Experimental Crystal Structure Determination, 2025, DOI: **10.5517/ccdc.csd.cc2mfp92**.
42 A. Chanda and S. K. Mandal, CCDC 2426225: Experimental Crystal Structure Determination, 2025, DOI: **10.5517/ccdc.csd.cc2mfpb3**.